Title

Geothermal production and reduced seismicity: Correlation and proposed mechanism

Authors

Cardiff, Michael
Lim, David D
Patterson, Jeremy R
et al.

Publication Date

2018

DOI

10.1016/j.epsl.2017.11.037

Peer reviewed

Earth and Planetary Science Letters 482 (2018) 470–477

Contents lists available at ScienceDirect

Earth and Planetary Science Letters

www.elsevier.com/locate/epsl

Geothermal production and reduced seismicity: Correlation and proposed mechanism

Michael Cardiff [a,*], David D. Lim [a], Jeremy R. Patterson [a], John Akerley [b], Paul Spielman [b], Janice Lopeman [b], Patrick Walsh [b], Ankit Singh [c], William Foxall [c], Herbert F. Wang [a], Neal E. Lord [a], Clifford H. Thurber [a], Dante Fratta [a], Robert J. Mellors [e], Nicholas C. Davatzes [d], Kurt L. Feigl [a]

[a] University of Wisconsin-Madison, United States
[b] ORMAT Technologies Inc., United States
[c] Lawrence Berkeley National Laboratory, United States
[d] Temple University, United States
[e] Lawrence Livermore National Laboratory, United States

ARTICLE INFO

Article history:
Received 22 July 2017
Received in revised form 14 November 2017
Accepted 15 November 2017
Available online 27 November 2017
Editor: P. Shearer

Keywords:
microseismicity
geothermal field
effective stress
correlation

ABSTRACT

At Brady Hot Springs, a geothermal field in Nevada, heated fluids have been extracted, cooled, and re-injected to produce electrical power since 1992. Analysis of daily pumping records and catalogs of microseismicity between 2010 and 2015 indicates a statistically significant correlation between days when the daily volume of production was at or above its long-term average rate and days when no seismic event was detected. Conversely, shutdowns in pumping for plant maintenance correlate with increased microseismicity. We hypothesize that the effective stress in the subsurface has adapted to the long-term normal operations (deep extraction) at the site. Under this hypothesis, extraction of fluids inhibits fault slip by increasing the effective stress on faults; in contrast, brief pumping cessations represent times when effective stress is decreased below its long-term average, increasing the likelihood of microseismicity.

1. Introduction

Fluid movement has long been associated with geologic faults (e.g., Hubbert and Rubey, 1959). In the Basin and Range Province, many geothermal fields coincide with systems of normal faults (e.g., Faulds et al., 2013). One such example is the geothermal field at Brady Hot Springs, northeast of Fernley, Nevada, USA (henceforth, "Brady"). Likewise, fluid pressure and seismicity on faults are associated. The effect of fluid pressure changes on the occurrence of seismic events has been recognized at a number of locations around the world, where fluid injections have been correlated with increases in seismic activity (Ellsworth, 2013). Injecting fluids in the subsurface perturbs the natural long-term stress state of a reservoir by increasing pore pressure; this increase in pore pressure results in a decrease in effective stress on faults, which can induce fault slip and associated seismic events. According to the "critical stress" hypothesis, even a small change in ambient pore pressure could facilitate fault slip via this process (Zoback and Harjes, 1997). "Triggering thresholds" associated with fault failure have been suggested as low as 0.01 MPa to 0.1 MPa (Gomberg et al., 2001), although there appears to be spatial variability in this sensitivity, which is a subject of current research. A standard conversion from pressure change to equivalent fluid height change would then suggest that a local change in water pressure equivalent to approximately 10 m of hydraulic head change has the potential to initiate seismic events at susceptible locations. Based on this mechanism, several studies at geothermal fields have correlated seismicity rates with changes to monthly injection rates (i.e., total injection from all wells) or net production rates (i.e., total extraction minus total injection via wells) (Brodsky and Lajoie, 2013; Johnson et al., 2016; Trugman et al., 2016).

The effect of pore pressure has been studied most prominently where ambient fluid pore pressure on faults is presumed to have been increased by fluid injection. However, ambient pore fluid pressure may also be raised by the opposite mechanism – i.e.,

* Corresponding author. Department of Geoscience, University of Wisconsin-Madison, 1215 W. Dayton St., Madison, WI 53706, United States.
E-mail address: cardiff@wisc.edu (M. Cardiff).

https://doi.org/10.1016/j.epsl.2017.11.037

a cessation of long-term extraction. Previous studies have noticed an apparent association between suspension of pumping operations and the occurrence of microseismicity at Brady (Davatzes et al., 2013a, 2013b). In this study, we analyze this association by quantifying the correlation in time and space, and we suggest a causal mechanism for the correlation. We present two data sets that support this correlation: a short-term record of pumping and pressure changes with minute-level information collected over a time interval of one month, and a comparable long-term daily record of pumping over a time interval of many years. We then correlate these data sets with records of local microseismicity to provide evidence that pressure perturbations associated with changes in pumping rates propagate quickly in the reservoir and consequently alter the effective stress on nearby faults. In comparing our study to earlier geothermal studies where correlations between operations and seismicity were evaluated, we note that our study takes advantage of: (1) Detailed records of the locations and daily timing of pumping rate changes (i.e., individual well flow rates); (2) Access to the positioning (depth, screen lengths) of all active site wells; and (3) Access to install a pressure observation well at the site during operations. These data have also been made available to the research community for further analysis on the Geothermal Data Repository (https://gdr.openei.org/) operated by the Department of Energy (DOE) Geothermal Technologies Office (Foxall, 2014, 2016; Lim, 2016, 2017).

2. Background

The site at Brady was initially developed in the 1920's for direct use (Lund, 1982). Then, in the 1950's, several parties performed exploratory drilling, and a geothermal power plant was established successfully in 1992, which has been operating continuously to the present day (Ettinger and Brugman, 1992). Since 2004, the site has been operated and monitored by ORMAT Technologies Inc. and its subsidiaries (henceforth "ORMAT") and produces clean electrical power from geothermal energy at a rate of roughly 10 MWe. In collaboration with DOE, universities, and national laboratories, ORMAT has made historical records of site operations available for scientific investigations, and has also allowed access and experimentation by scientific researchers, in an effort to better understand the geothermal resource. The short-term data presented in this work represent the results of one such experiment, PoroTomo (Poroelastic Tomography), carried out in March 2016, during which ORMAT allowed access and use of the site for hydrologic and geophysical investigations. Longer-term data sources presented in this work represent other project efforts, including the "Brady EGS" and the "InSAR-MEQ" Projects, both funded by DOE.

The study area at Brady is located in the Basin and Range Province of western Nevada, USA approximately 80 km northeast of Reno along Interstate Highway 80. This region is characterized by a transtensional tectonic regime, and is dominated by normal faults striking SW–NE (Fig. 1). In the vicinity of Brady, Faulds and colleagues (Faulds et al., 2006, 2010) have mapped surface fault and formation boundaries, collected seismic reflection profiles, recorded gravity data, and examined well cores. Building on these observations, several studies have interpreted and integrated existing data sources to develop 3-D geologic models for the subsurface structure beneath Brady (Jolie et al., 2015; Siler et al., 2016; Witter et al., 2016). These geologic models show two distinct sets of normal faults, with one set dipping to the NW and the other to the SE. The faults cut through a series of sedimentary units of Pliocene to Miocene age and through volcanic, intrusive igneous, and metamorphic rock layers of Miocene to Mesozoic age. The damage zones associated with this intricate network of faults form the geothermal resource tapped by production wells at Brady (Ali et al., 2016; Davatzes et al., 2013a;

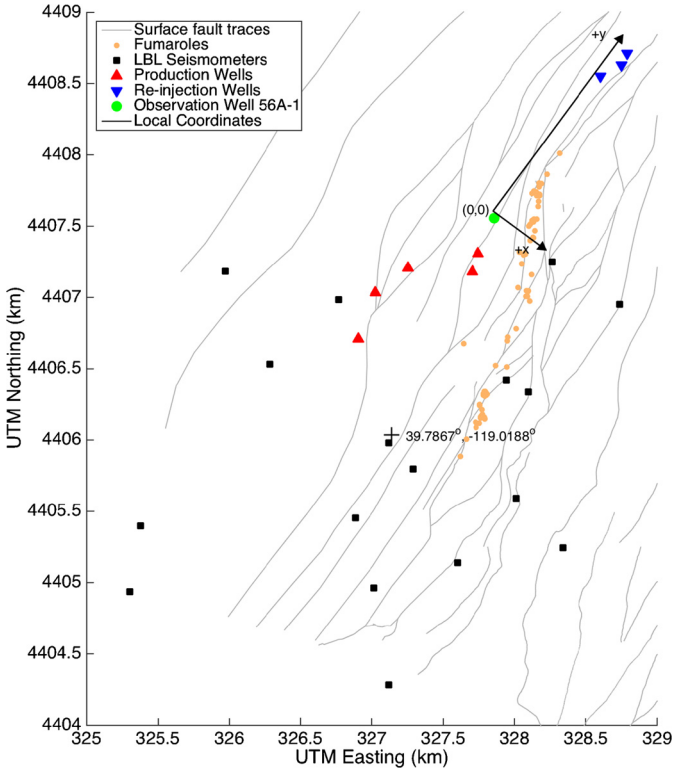

Fig. 1. Local map of Brady Hot Springs showing well and seismometer locations, surface fault expressions (Faulds et al., 2010), and local coordinate scheme, as used in Fig. 3. Fiducial point represents latitude and longitude for Brady well 15–12.

Laboso and Davatzes, 2016; Siler et al., 2016). These studies suggest that the geothermal reservoir is partially recharged by highly permeable conduits along faults, which channel fluids from shallow aquifers to the deep geothermal reservoir.

The operational infrastructure at Brady includes several deep production wells that range from approximately 400 m to 1800 m below land surface (bls). Insulated pipes carry super-heated brine to the Brady power plant, where geothermal energy is extracted through a dual-flash system (the Ormat Energy Converter) that drives a set of turbines. After heat extraction, the cooled water is recycled back into the subsurface. Most of the cooled fluid flows into three much shallower injection wells (~200 m bls) located approximately 2 km northeast of the plant, while a small proportion is redirected to a similarly shallow offsite injection well approximately 6 km to the south of the geothermal plant in a separate basin. A negligible amount of brine is pumped for direct use by a nearby vegetable drying plant.

3. Data

3.1. Long-term pumping records

Daily extraction and injection volumes at the Brady site have been continuously recorded by ORMAT and were supplied to the PoroTomo project for dates between 2004 January 1 to 2016 March 28. The data set includes: (1) daily observation of extraction and injection flow rates in gallons per minute, recorded primarily through manual gauge readings; and (2) a record of the daily time online, in minutes, for each well. For the time interval coincident with the seismic event catalogs discussed later, the database contains a complete daily record, although the time series contains several gaps before 2008. To find the total daily extracted and injected volumes, we multiplied the flow rate recorded by the number of minutes of operation for each well and converted the

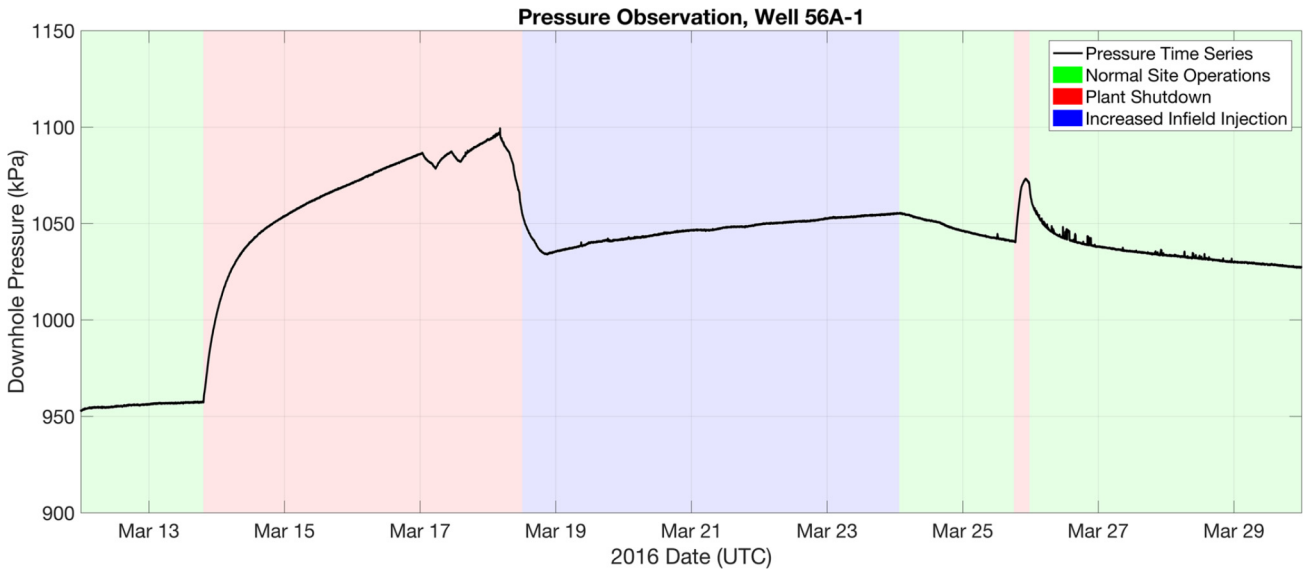

Fig. 2. Pressure changes measured at well 56A-1 during PoroTomo experiment. Colored boxes delineate phases of the PoroTomo experiment. A brief unplanned site shutdown on 2016 March 25 UTC is also delineated.

resulting quantity in gallons per day to SI units of cubic meters per day.

3.2. Pumping and pressure records during the PoroTomo experiment

In 2016, pressure transducers were installed in three favorably-located observation wells as part of the "PoroTomo" project (Feigl and PoroTomo Team, 2017). This project is a collaborative effort to characterize the critical reservoir properties in a geothermal system. The PoroTomo field experiment consisted of a month-long field campaign in March 2016 that included four stages. During Stage 1 ("normal operations"), pumping at all production and injection wells was consistent with normal site conditions. In this configuration, the production wells extract hot brine from the southern portion of the geothermal field. After passing through the heat exchangers in the power plant, most of the brine (∼80%) is recycled into shallow injection wells at the northeastern edge of the field. A small percentage (∼20%) is re-directed off-site to a well 6 km away in a neighboring basin. During Stage 2 ("site shutdown"), the power plant was taken offline and all production and injection activities ceased at all wells. At the beginning of Stage 3 of the experiment ("increased injection"), all production and injection wells were brought back into operation with the exception of the far-field injection well, which had its valve closed, resulting in all cooled water being re-injected at the northeastern end of the site. Finally, during Stage 4, normal operations of the site resumed.

During the PoroTomo field campaign (2016 March 11–2016 March 28), pumping rates were recorded at a rate of 1 sample/minute, and pressure changes were monitored by the pressure transducers installed in the three on-site wells, likewise sampling at a rate of 1 sample/minute. Fig. 2 shows the pressure changes measured at well 56A-1, the observation well closest to the production wells (Lim, 2016, 2017).

3.3. Long-term seismic event catalog

In 2010, a network of seismometers was installed at Brady (Foxall, 2014; Nathwani et al., 2011). Microseismic events are automatically detected by this array using automated triggering and are then manually reviewed. Initial hypocenter estimates for these events are automatically estimated using a 1-dimensional velocity model. The events recorded between 2010 and 2015 have been re-analyzed by scientists at Lawrence Berkeley National Laboratory (LBL), who carried out simultaneous inversion to estimate event times and relocated hypocenters, along with 3-dimensional P- and S-wave velocity models (Foxall, 2016). The first event in this relocated long-term catalog is dated 2010 November 13, and the last event analyzed using this approach occurred on 2015 March 24. None of the events in this catalog were felt by humans. With the exception of a single moment magnitude (M_w) 2.2 event in November 2010, no event in this re-analyzed catalog exceeded magnitude M_w 2.0. The detection threshold within the array is estimated at about $M_w \sim -1.0$. Based on Gutenberg–Richter plots, this catalog is estimated to be complete to approximately $M_w \sim 0.5$. All event hypocenters from this catalog are shown spatially in Fig. 3, along with the locations of site wells. Absolute location errors for these events have been determined statistically, and are estimated to be less than 500 m for 95% of the epicentral locations and less than 500 m for 80% of the depth estimates. Location errors are associated with error in arrival time picks as well as with sensitivity to the starting velocity model used during simultaneous inversion. In Fig. 3, the open intervals of wells at the Brady site are highlighted as sections of thicker black lines – we note that these intervals appear to have similar depths to the location of event hypocenters, suggesting that a zone tapped for geothermal heat is associated with faulting at this interval. The apparent dip of the seismic event cloud also agrees with interpretations of subsurface fault geometry produced by Jolie et al. (2015).

3.4. PoroTomo seismic event catalog

The seismic network at Brady was operational throughout the duration of the PoroTomo experiment and continues to record microseismic events near Brady. As described above, events recorded by this network are auto-picked in near-real time and hypocenters are calculated automatically, which are displayed on the LBL induced seismicity website (LBL, 2016). These events are manually screened and re-picked on a weekly basis, with updated magnitudes and hypocenters posted to the website. This catalog lists five microseismic events that occurred during the PoroTomo experiment, all of which are below M_w 1.0. These events are shown, along with the long-term catalog, as a separate color in Fig. 3. Estimated absolute location errors for these events are less than 200 m for the epicenter and less than 600 m for depth.

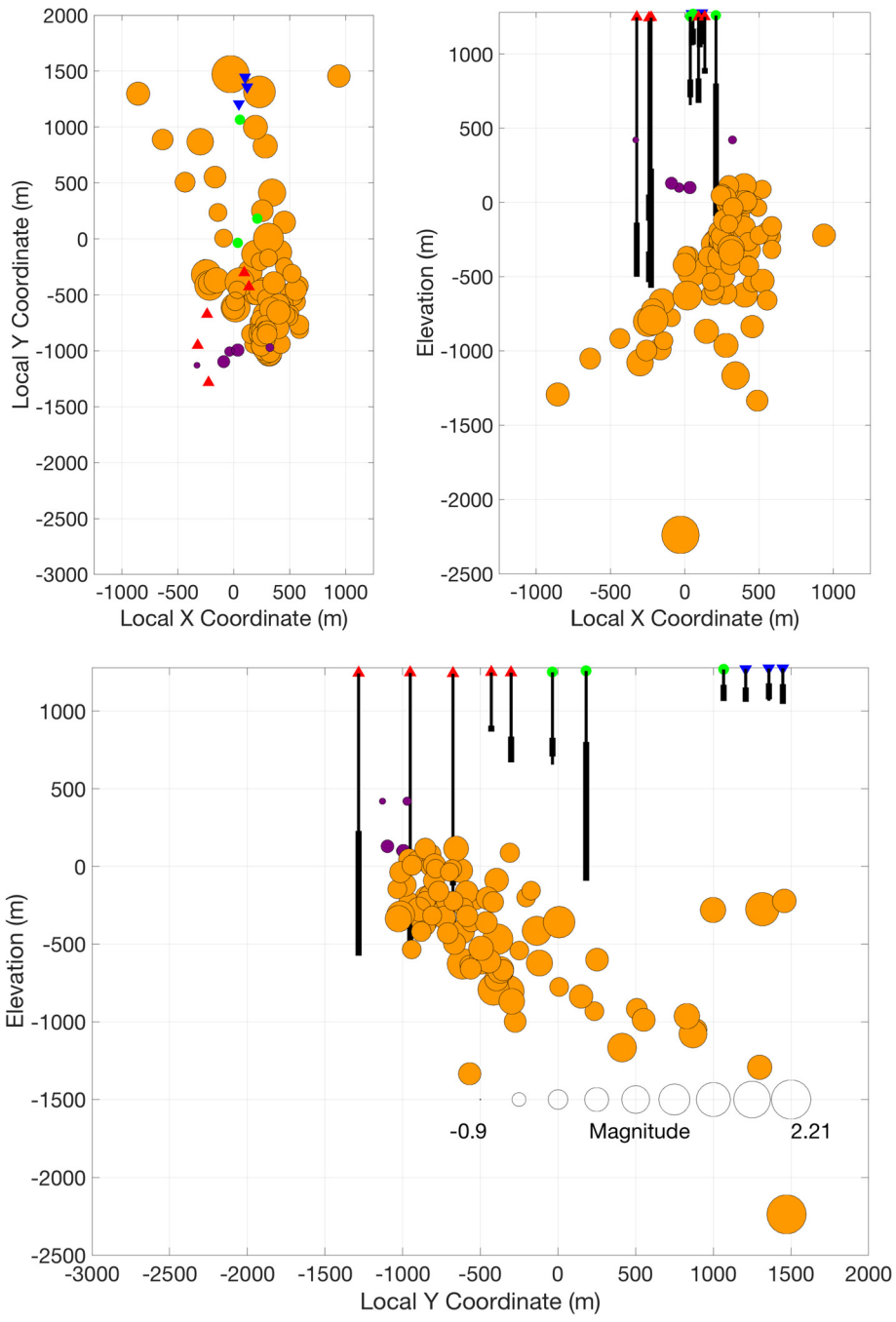

Fig. 3. Views of Brady subsurface, showing horizontal map view (top left), projection to a vertical plane striking NE (top right), and projection to a vertical plane striking NW (bottom). Orange circles show hypocentral locations in the long-term catalog, spanning dates from November 2010 to March 2015 (Foxall, 2016). Purple disks show hypocentral locations from the short-term catalog, spanning March 2016 dates of the PoroTomo experiment. Black lines show wells, with thicker segments representing intervals that are open to the surrounding formation. Red triangles denote production wells; blue, injection wells; green, observation wells. All elevations are represented as height above WGS84 ellipsoid.

4. Analysis

4.1. Analysis of hydraulic properties

We assume that fluid flow at the Brady site occurs primarily along two-dimensional (roughly planar) conduits associated with fault zone permeability, since the host rock adjacent to production wells consists largely of Miocene volcanic deposits, ash-flow tuffs, and sedimentary rocks that presumably have low intrinsic permeability (Davatzes et al., 2013a; Laboso and Davatzes, 2016; Siler et al., 2016). Likewise, the correspondence between screened intervals for successful (operating) pumping wells, microseismic event hypocenters, and an interpreted fault plane suggests that heated fluids are carried predominantly along fault damage zones, and may be associated primarily with one or a few fault zones. Assuming a conceptual model in which flow occurs dominantly along a single faulted zone (i.e., a two-dimensional flow geometry) within largely impermeable host rock, the fluid pressure increase following the interruption of long-term extraction can be calculated as (e.g., Theis, 1935):

$$\Delta p(r,t) = \frac{Q\rho g}{4\pi T} W\left[\frac{r^2 S}{4Tt}\right] \tag{1}$$

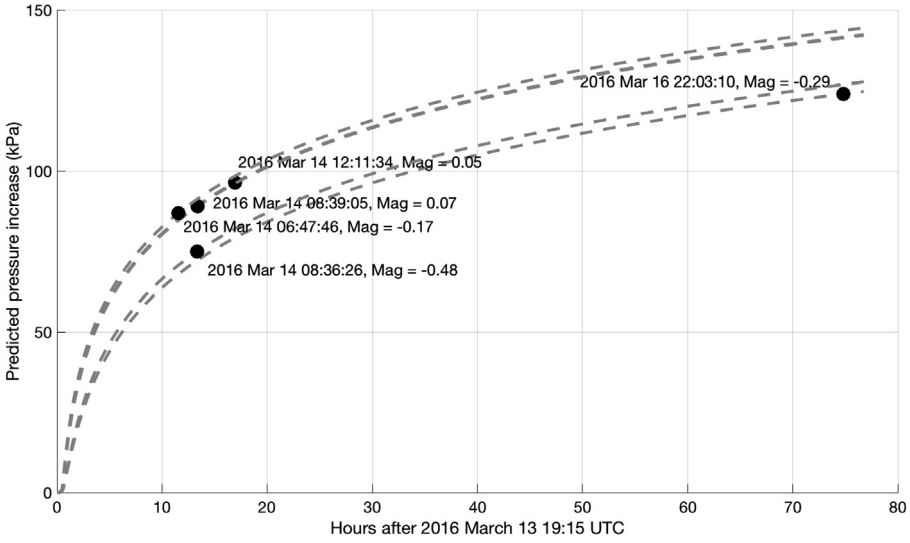

Fig. 4. Modeled pressure change over time at locations of microseismic events, with actual event times highlighted. Shutdown of pumping at site extraction wells began at 2016 March 13 19:15 UTC.

where Δp [kg/(m s^2)] is the pressure change at radius r [m] away from the pumping location, t [s] is the time since extraction stopped, Q [m^3/s] is the long-term volumetric flow rate at the extraction well, ρ [kg/m^3] is the density of the extracted fluid, g [m/s^2] is the acceleration of gravity, T [m^2/s] is the transmissivity of the fault zone, S [–] is the fault zone storativity, and $W(\cdot)$ is the so-called well function, also known as the exponential integral (dimensionless, [−]). The two reservoir parameters T and S are by far the greatest source of uncertainty in modeling the reservoir response, as they vary over several orders of magnitude in natural systems.

We estimate transmissivity T and storativity S for the Brady site using pressure change data from well 56A-1 during the time interval of Stage 2 when all pumping was suspended, as delimited by red shading in Fig. 2. Specifically, we focus on the times between 13 March 2016 19:15 UTC and 17 March 2016 00:00 UTC, since the later portion of Stage 2 included short intervals of pumping as wells were tested before the geothermal plant was brought back online. To account for the different locations and timings of extraction shutdowns at the five production wells, we superposed the analytical solutions to equation (1) for each extraction well to obtain the net pressure change at well 56A-1. In order to estimate the reservoir parameters T and S, we employ a nonlinear least-squares objective function that minimizes the sum of squared residuals (observed minus simulated pressure changes), which is solved via nonlinear optimization with the Nelder–Mead simplex algorithm as implemented in MATLAB. Since the optimization is nonlinear, the dependence of the obtained parameter estimates on the starting guess was assessed by trying multiple initial parameter estimates, spanning a range of several orders of magnitude. All optimizations converged to the same minimum misfit solution, indicating that the optimization had converged to a global minimum. Through this parameter estimation, we obtain a transmissivity $T = 1.3 \times 10^{-2}$ m^2/s and storativity $S = 1.8 \times 10^{-4}$ [−], or a hydraulic diffusivity of $D = T/S = 71.6$ m^2/s. Residuals associated with the data fit from this parameter estimation (observed minus modeled pressure change values) have a root mean squared error (RMSE) of 1.6 kPa, which is near the sensor accuracy of 1 kPa specified by the pressure transducer manufacturer (K10 Quartz by Kuster Company). Earlier site reports that analyzed flow tests following well drilling obtained similar estimates of reservoir diffusivity, adding confidence to these estimates. Using linearized propagation of variance (see, e.g., Aster et al., 2005), the uncertainty in hydraulic diffusivity is estimated to be less than 10%.

4.2. Microseismicity during PoroTomo experiment

During Stage 2 of the PoroTomo experiment, when all pumping operations were suspended, five microseismic events were detected. Each of these events occurred during the time interval between 14 March 2016 19:15 UTC and 17 March 2016 00:00 UTC when no pumps were operating. No further events were detected by the seismic network until November 2016. The magnitude for the five events ranged from −0.48 M_w to 0.07 M_w.

One possible explanation for these and other microseismic events involves the change in pressure caused by the temporary suspension of pumping for maintenance at the geothermal plant. Under this hypothesis, the fault system at Brady has adapted to a “background” stress state in which pore pressure is locally reduced due to extraction by deep production wells. The interruption of this extraction then represents a relative increase in local pore pressure above these background values, and a concomitant decrease in the local effective normal stress on faults. We note that at observation well 56A-1, the interruption of extraction contributes to a pressure change of greater than 100 kPa (0.1 MPa) roughly one day after extraction ceased (Fig. 2). The open interval of this observation well is located approximately 270 m from the closest extraction interval, suggesting that these large pressure changes propagate through the reservoir quickly.

To investigate whether this propagation of pressure change could explain microseismicity at Brady, we apply the same analytic model described above in equation (1), along with the previously estimated values of transmissivity T and storativity S, to calculate the pressure changes that would be expected at the time and hypocentral location of each of the five detected microseismic events. Distances from extraction intervals of site wells to hypocenters ranged between roughly 350 m and 1,100 m, with four of the five events occurring less than 20 hrs after extraction was suspended. The final event on 2016 March 16 occurred more than 70 hrs after extraction was suspended, but before extraction was resumed. In Fig. 4, we show the expected pressure change at each of the hypocentral locations following the site shutdown, using the previously obtained hydraulic diffusivity of $D = 71.6$ m^2/s. The occurrences of the actual microseismic events are plotted on top of these pressure change curves in Fig. 4 to highlight the magnitude of pressure change expected at each hypocentral location and time. Each of the five events occurs when the simulated increase in pressure is between 0.07 and 0.13 MPa. Other analyses were performed

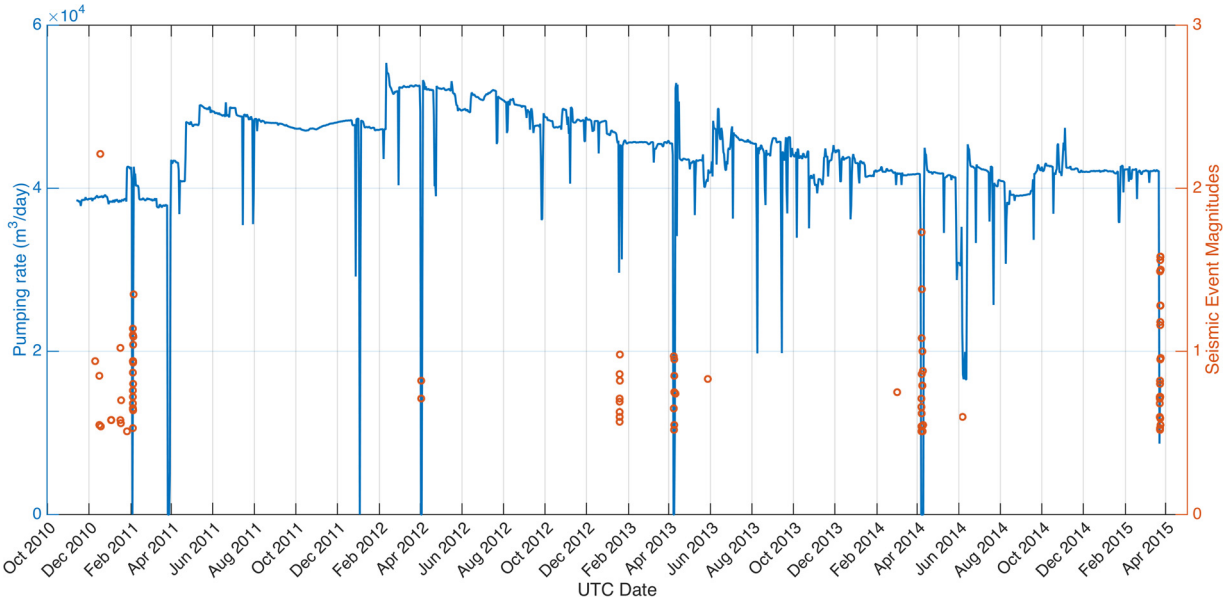

Fig. 5. Comparison between long-term Brady site extraction rates (blue line) and event times from long-term microseismic catalog (orange circles), for microseismic events with $M_w > 0.5$. (For interpretation of the colors in this figure, the reader is referred to the web version of this article.)

on these pressure change calculations, considering a range of diffusivity estimates associated with the uncertainty discussed earlier. However, the result of these uncertainties on predicted pressure changes was minimal, and is thus not presented here.

4.3. Long-term correlation analysis

Next, to further test the hypothesis that the extraction of fluids inhibits slip by increasing the effective stress within the rock, we analyze the correlation in space and time between the long-term pumping records and the seismic event catalog, over the 5-yr time interval coincident with the long-term catalog. Fig. 3 shows the locations of the estimated hypocenters and the wells at Brady, including the five events in the PoroTomo seismic event catalog in purple. Spatially, most of the estimated hypocentral locations fall near a plane dipping northwest and striking northeast, with depths similar to those targeted by the production wells, again suggesting a spatial connection to fluid extraction. Notably, none of the cataloged hypocenters occur in the vicinity of shallow injection wells at Brady. Seismicity has been correlated with injection at other geothermal fields, where increased fluid pressure and corresponding decreased effective normal stress on faults represents a proposed mechanism (see, e.g., Trugman et al., 2016). At Brady, the injection of water at shallow depths (where overburden is lower) may limit this effect. Likewise, the possibility of near-surface porous media-driven flow rather than fault-controlled flow could help to limit pressure changes nearer to the land surface. Cold water injection has also been proposed as a mechanism for producing microseismicity at geothermal sites (via cooling-induced thermal stresses) (e.g., Majer et al., 2007). However, this process does not appear likely at Brady given the spatial distribution of microseismicity.

As with the events in the short-term PoroTomo microseismic catalog, we hypothesize that the occasional suspensions of fluid extraction during routine plant maintenance increase fluid pressure along this plane, which allows fault stress releases and provides a mechanism for the associated microseismicity measured by longer-term seismic catalogs. To facilitate visual correlation of this temporal trend, Fig. 5 shows the two long-term time series between 2010 and 2015: the daily extracted volume (blue curve) along with the time and magnitudes of the microseismic

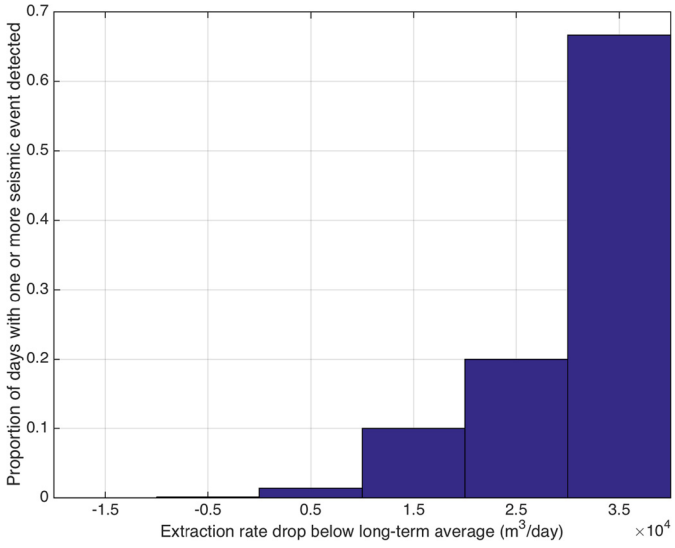

	Days with event detected	Days with no event detected	**Totals**
Extraction substantially reduced	10	15	**25**
Normal operations	14	1555	**1568**
Totals	**24**	**1570**	**1594**

Fig. 6. Top – relationship between daily extraction rate drop and proportion of monitored days with 1 or more seismic events detected with $M_w > 0.5$. Bottom – contingency table using a threshold of 2.2×10^4 m^3/day below the long-term average pumping.

events (orange circles) in the seismic catalog (Foxall, 2016). The vast majority of the microseismic events occurred on days when the production rate was zero, indicating that the extraction was suspended, presumably for maintenance at the power plant. Conversely, when daily extraction is at or above its long-term average, daily microseismicity is rare (less than 1% of the observed days), as shown in Fig. 6 (top).

To quantify the correlation, one approach is to define a threshold. If the daily extraction rate was less than 50% of the average long term pumping rate (i.e., reduced by more than 2.2 ×

10^4 m^3/day below the long-term average), then we consider the extraction to have been substantially reduced on that day. Otherwise, we consider the day as one of normal operations. Fig. 6 (bottom) shows a contingency table using this threshold. For example, no seismic event was detected on 1548 of the 1568 days when the production pumps were operating normally. Fisher's nonparametric test for contingency tables tests the null hypothesis of conditional independence, i.e., that there is no significant difference in the variable distribution ("event detected") between the rows (describing the pumping status) (Fisher, 1922). For the data presented, the value of the test statistic (the odds ratio) is 74.0, where an odds ratio of unity implies independence. For an odds ratio of 74.0, the associated p-value is well below a 1% threshold ($P \sim 10^{-13}$), meaning that the null hypothesis of independence can be rejected with greater than 99% confidence. We therefore infer a strong correlation between normal pumping operations and reduced local microseismicity.

5. Discussion & conclusions

In the geothermal field at Brady Hot Springs, we have estimated the hydraulic diffusivity to be on the order of 70 m^2/s. We thus infer that after 24 hrs or more, the fluid pressure change resulting from a suspension of pumping operations is on the order of 0.1 MPa at locations ~1 km from the production wells. Microseismic events have been monitored at Brady and appear to be near the location of existing production (extraction) wells. The days between 2010 and 2015 when normal operations extracted fluids at or above the long-term average rate correlate significantly with time intervals of few or no detectable microseismic events. We infer that the effective stress on faults during normal operations was higher, which suppressed microseismicity. Conversely, shutdowns in site operation represent times when the effective normal stress on faults is below long-term averages, allowing microseismicity to occur.

Acknowledgements

The authors wish to acknowledge the generous contributions of ORMAT Technologies Inc., who provided site access for installation of high-frequency pressure transducers as well as historical (daily) data on pumping records at the Brady Hot Springs geothermal field. Field assistance throughout the PoroTomo experiment by Michelle Robertson (LBL) is also gratefully acknowledged. Data products for this study were accessed through the Induced Seismicity Data Website at the Lawrence Berkeley National Laboratory, which is supported by the U.S. DOE Office of Geothermal Technology. This research was supported by grants DE-EE0005510 and DE-EE0006760 from the Geothermal Technologies Office of the U.S. Department of Energy. The data used are listed in the references, tables, and can be found on the Geothermal Data Repository at: https://gdr.openei.org/, keyword: PoroTomo.

Appendix A. Supplementary material

Supplementary material related to this article can be found online at https://doi.org/10.1016/j.epsl.2017.11.037.

References

Ali, S.T., et al., 2016. Time-series analysis of surface deformation at Brady Hot Springs geothermal field (Nevada) using interferometric synthetic aperture radar. Geothermics 61, 114–120.

Aster, R.C., Borchers, B., Thurber, C.H., 2005. Parameter Estimation and Inverse Problems, 301 pp.

Brodsky, E.E., Lajoie, L.J., 2013. Anthropogenic seismicity rates and operational parameters at the Salton Sea Geothermal Field. Science 341 (6145), 543–546.

Davatzes, N.C. Feigl, K.L. Mellors, R.J. Foxall, W. Wang, H.F. Drakos, P., Preliminary Investigation of Reservoir Dynamics Monitored Through Combined Surface Deformation and Micro-Earthquake Activity: Brady's Geothermal Field, Nevada (Sgp-Tr-198), 2013. Paper presented at Proceedings, Thirty-Eighth Workshop on Geothermal Reservoir Engineering Stanford University, Stanford, California, February 11–13, 2013.

Davatzes, N.C. Ali, T. Mellors, R.J. Foxall, W. Wang, H.F. Feigl, K.L. Drakos, P. Zemach, E., Contrasts Between Deformation Accommodated by Induced Seismic and Aseismic Processes Revealed by Combined Monitoring of Seismicity and Surface Deformations: Brady Geothermal Field, Nevada, USA, 2013. Paper presented at Fall Meeting American Geophysical Union, San Francisco.

Ellsworth, W.L., 2013. Injection-induced earthquakes. Science 341 (6142), 1225942.

Ettinger, T., Brugman, J., 1992. Brady hot springs geothermal power plant. In: 14th New Zealand Geothermal Workshop, Edited. New Zealand, pp. 89–91.

Faulds, J.E., Coolbaugh, M.F., Vice, G.S., Edwards, M.L., 2006. Characterizing structural controls of geothermal fields in the northwestern Great Basin: a progress report. Trans., Geotherm. Resour. Counc. 30, 69–76.

Faulds, J.E., Hinz, N.H., Dering, G.M., Siler, D.L., 2013. The hybrid model—the most accommodating structural setting for geothermal power generation in the Great Basin, Western USA. Trans., Geotherm. Resour. Counc. 37, 3–10.

Faulds, J.E., Coolbaugh, M.F., Benoit, D., Oppliger, G., Perkins, M., Moeck, I., Drakos, P., 2010. Structural controls of geothermal activity in the northern Hot Springs Mountains, western Nevada: the tale of three geothermal systems (Brady's, Desert Peak, and Desert Queen). Trans., Geotherm. Resour. Counc. 34, 675–683.

Feigl, K.L. PoroTomo Team, Overview and Preliminary Results from the PoroTomo project at Brady Hot Springs, Nevada: Poroelastic Tomography by Adjoint Inverse Modeling of Data from Seismology, Geodesy, and Hydrology, 2017. Paper presented at 42nd Workshop on Geothermal Reservoir Engineering, Stanford University, Stanford, CA, USA.

Fisher, R.A., 1922. On the interpretation χ^2 from contingency tables, and the calculation of P. J. R. Stat. Soc. 85 (1), 87–94.

Foxall, W., 2014. Brady's geothermal field seismic network metadata [data set]. Retrieved from https://doi.org/10.15121/1166944. http://gdr.openei.org/submissions/469, 2014.

Foxall, W., 2016. PoroTomo subtask 3.1 Meq relocations & 3D velocity models 30 June 2015 [data set]. Retrieved from https://gdr.openei.org/submissions/493. https://doi.org/10.15121/1196282, 2016.

Gomberg, J., Reasenberg, P.A., Bodin, P., Harris, R.A., 2001. Earthquake triggering by seismic waves following the Landers and Hector Mine earthquakes. Nature 411 (6836), 462–466.

Hubbert, M.K., Rubey, W.W., 1959. Role of fluid pressure in the mechanics of overthrust faulting. Bull. Geol. Soc. Am. 70, 115–166.

Johnson, C.W., Totten, E.J., Bürgmann, R., 2016. Depth migration of seasonally induced seismicity at The Geysers geothermal field. Geophys. Res. Lett. 43 (12), 6196–6204.

Jolie, E., Moeck, I., Faulds, J.E., 2015. Quantitative structural–geological exploration of fault-controlled geothermal systems—a case study from the Basin-and-Range Province, Nevada (USA). Geothermics 54, 54–67.

Laboso, R.C. Davatzes, N.C., Fault-Controlled Damage and Permeability at the Brady Geothermal System, Nevada, USA (SGP-TR-209), 2016. Paper presented at 41st Workshop on Geothermal Reservoir Engineering Stanford University, Stanford, California, February 22–24, 2016.

LBL, 2016. EGS: Interactive, Real-Time Map of Earthquakes at Bradys Hot Springs. Edited.

Lim, D., 2016. PoroTomo subtask 6.8—Brady well coordinates and observation sensor depths [data set]. Retrieved from https://gdr.openei.org/submissions/828. https://doi.org/10.15121/1261986, 2016.

Lim, D., 2017. Porotomo: analysis of pressure data [data set]. Retrieved from https://gdr.openei.org/submissions/917. https://doi.org/10.15121/1367912, 2017.

Lund, J.W., 1982. Geothermal vegetable dehydration at Brady's Hot Springs. Geo-Heat Cent. Q. Bull. 7 (2), 14–16.

Majer, E.L., Baria, R., Stark, M., Oates, S., Bommer, J., Smith, B., Asanuma, H., 2007. Induced seismicity associated with enhanced geothermal systems. Geothermics 36 (3), 185–222.

Nathwani, J. Majer, E. Boyle, K. Rock, D. Peterson, J. Jarpe, S., DOE Real-Time Seismic Monitoring at Enhanced Geothermal System Sites, 2011. Paper presented at Thirty-sixth Workshop on Geothermal Reservoir Engineering.

Siler, D.L. Hinz, N.H. Faulds, J.E. Queen, J., 3D Analysis of Geothermal Fluid Flow Favorability: Brady's, Nevada, USA, 2016. Paper presented at Proceedings, 41st Workshop on Geothermal Reservoir Engineering Stanford University, Stanford, California, February 22–24, 2016 SGP-TR-209.

Theis, C.V., 1935. The relation between lowering the piezometric surface and the rate and duration of discharge of a well using ground water storage. Eos 16, 519–524.

Trugman, D.T., Shearer, P.M., Borsa, A.A., Fialko, Y., 2016. A comparison of long-term changes in seismicity at The Geysers, Salton Sea, and Coso geothermal fields. J. Geophys. Res., Solid Earth 121 (1), 225–247.

Witter, J.B., Siler, D.L., Faulds, J.E., Hinz, N.H., 2016. 3D geophysical inversion modeling of gravity data to test the 3D geologic model of the Bradys geothermal area, Nevada, USA. Geotherm. Energy 4 (1), 14.

Zoback, M.D., Harjes, H.-P., 1997. Injection-induced earthquakes and crustal stress at 9 km depth at the KTB deep drilling site, Germany. J. Geophys. Res., Solid Earth 102 (B8), 18477–18491.